Tailoring infrared optical properties with superlattices of superlattices

G. T. Einevoll and L. J. Sham
Department of Physics, University of California at San Diego, La Jolla, California 92093-0319
(Received 15 April 1992)

The concept of superlattices of superlattices (SOS's) is introduced to tailor infrared optical properties in semiconductor devices. SOS structures are constructed by alternating two different superlattices. By describing the separate superlattice sections in terms of their miniband edges and miniband-edge effective masses, and by using these parameters as input in a nested effective-mass theory, a transparent connection between the choice of material parameters and device properties is obtained. As one example of application we use the concept to propose SOS infrared detectors with more flexibility and potentially better performance compared to photodetectors based on conventional superlattices. In another example the idea is applied to lateral superlattices. It is shown that the desirable features of the SOS structures are robust against disorder in the layer thicknesses.

I. INTRODUCTION

The utilization of intersubband absorption in quantum wells and superlattices in making fast and efficient infrared photodetectors (IP's) has recently attracted much interest.[1–16] Although most studies have been on $GaAs/Al_xGa_{1-x}As$ heterostructures,[1–11] other material systems like $In_xGa_{1-x}As/InP$,[12,13] $In_xAl_{1-x}As/In_xGa_{1-x}As$,[14] and SiGe/Si (Refs. 15 and 16) have also been investigated. In the original work of Levine *et al.*,[1] the IP was based on intersubband transitions between the ground state and first excited state in $GaAs/Al_xGa_{1-x}As$ quantum wells with wells wide enough to contain two bound states. The photoexcited electron then had to tunnel through the $Al_xGa_{1-x}As$ barrier to escape the well, and quite thin barriers ($L_b \sim$ 95 Å) were necessary in order to obtain a photocurrent. With narrow wells only one state is bound in the well, and the final state in the photoabsorption process is in the continuum above the barrier. This gives broader absorption lines, but the photoelectrons can be collected without tunneling, and good detectivities can be achieved.[2] Since in this case the electron transport does not rely on tunneling, the barriers can also be made very thick to lower the undesirable dark tunneling current from electrons in the quantum-well ground state. (The electrons are only confined in the growth direction, and each state in the quantum well thus gives rise to a 2D subband.) With very thin barriers the coupling between adjacent wells may be so strong that it is more appropriate to consider a miniband in the growth direction than a set of isolated quantum-well states. Gunapala, Levine, and Chand[3] recently demonstrated such miniband-to-miniband absorption and photoconduction for the case where the second miniband is above the top of the barriers, but structures with both minibands below the barrier have also been considered.[4,5]

In this paper we present superlattices of superlattices (SOS's), which are structures consisting of periodically alternating superlattices, as an additional way of tailoring electronic and optical properties in infrared devices. The principle is illustrated in Fig. 1. The basic building blocks, consisting of single slabs of well material symmetrically sandwiched between two slabs of barrier material [Fig. 1(a)], are put together to make the desired structure [Fig. 1(b)]. Due to the numerous material parameters in such structures it is not unexpected that they offer flexibility in tailoring device properties. A major problem is that although exact transcendental equations for the single-particle states in SOS are straightforward to obtain, the connection between the choice of material parameters and the positions of the electronic levels is not transparent. To get a handle on the connection it is very useful to describe each superlattice section of the SOS in terms of their miniband structure and associated miniband-edge effective masses. Just as most of the properties of regular superlattices can be understood in terms of position-dependent band edges and band-edge effective masses, most of the properties of the SOS can be understood in terms of position-dependent miniband edges and the associated miniband-edge effective masses. In fact this *nested* effective-mass theory offers more than a qualitative description: in many situations of physical interest it provides a quantitatively accurate description.

Since our aim is to promote the use of the SOS concept in device design, we also consider effects from disorder in layer thicknesses. From calculations of absorption spectra on concrete examples, it is shown that the desirable features of the SOS structures are robust against this type of imperfection.

In Sec. II the calculational method is described. In Sec. III the SOS concept is applied to conventional superlattices to tailor the operating frequency and spectral width of the device. Lateral superlattices have recently attracted interest[17] and have been proposed for infrared devices.[18] In Sec. IV we apply the SOS idea to such superlattices. A short summary and discussion are given in Sec. V.

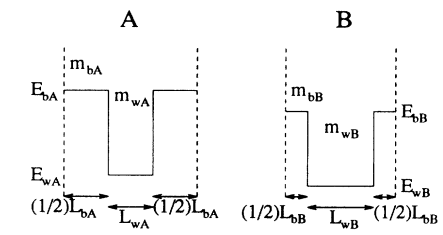

(a)

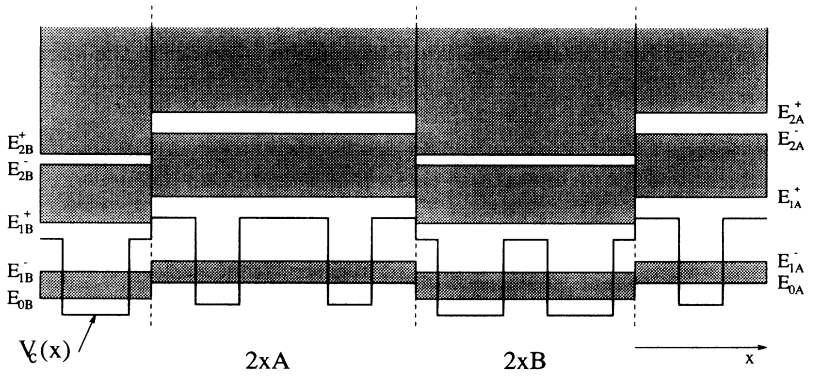

(b)

FIG. 1. The basic building blocks A and B (a) put together in a 2×2 SOS structure (b). In (b) the conduction-band edge profile $V_c(x)$ and the lowest minibands of the constituent superlattices are shown. The five lowest miniband edges of the two superlattices are marked.

II. THEORY

Within the standard effective-mass approximation electronic states in the vicinity of the conduction-band edge are described by[19]

$$\left[-\frac{\hbar^2}{2}\frac{d}{dx}\frac{1}{m(x)}\frac{d}{dx}+V_c(x)\right]\phi(x)=E\phi(x)\,. \tag{1}$$

Here the effective mass $m(x)$ takes on the values m_{bA}, m_{wA}, m_{bB}, and m_{wB} according to the position in the SOS. Correspondingly, $V_c(x)$ takes on the values E_{bA}, E_{wA}, E_{bB}, and E_{wB}. For the moment we do not consider the electronic motion in the yz plane, i.e., perpendicular to the growth direction. The boundary conditions at the material interfaces corresponding to the kinetic operator in Eq. (1) are continuity of ϕ and of ϕ'/m.[19] With the use of the standard transfer-matrix technique,[20] and by imposing Bloch boundary conditions at the boundary between two SOS unit cells, it is straightforward to evaluate the SOS eigenstates.

To utilize the more transparent nested effective-mass approximation we need the miniband edges and corresponding effective masses for the superlattices in the SOS. The condition for superlattice eigenstates is[19]

$$\cos(q_wL_w)\cos(q_bL_b) - \frac{1}{2}\left(\frac{m_b}{m_w}\frac{q_w}{q_b}+\frac{m_w}{m_b}\frac{q_b}{q_w}\right)\sin(q_wL_w)\sin(q_bL_b) = \cos[k_x(L_w+L_b)]\,. \tag{2}$$

Here k_x is the miniband wave vector, and q_w and q_b, which can be both real and imaginary, are connected with the energy E via $E=E_w+\hbar^2q_w^2/2m_w$ and $E=E_b+\hbar^2q_b^2/2m_b$. The miniband edges occur when the left side of Eq. (2) is $+1$ or -1. Although these miniband edges are easily obtained numerically, approximate expressions which show dependencies on material parameters explicitly are in many cases more useful. An expansion of Eq. (2) in small offsets, $V_{\rm off}\equiv E_b-E_w$ (on the scale of $\hbar^2/2m_iL_i^2$, $i=w,b$) yields the following approximate expressions for the miniband edges:[21]

$$E_0=E_w+\frac{L_b}{L_w+L_b}V_{\rm off}-\frac{L_w^2L_b^2(m_wL_w+m_bL_b)}{6\hbar^2(L_w+L_b)^3}V_{\rm off}^2 \tag{3}$$

for the lowest miniband edge, and

$$E_n^{\pm} = E_w + \frac{L_b}{L_w + L_b} V_{\text{off}} + \frac{\hbar^2 n^2 \pi^2}{2(L_w + L_b)(m_w L_w + m_b L_b)} \pm \frac{n\pi G}{2\sqrt{2}} \left| \frac{(m_b - m_w)\hbar^2}{m_b m_w (L_w + L_b)^2} + \frac{2V_{\text{off}}}{n^2\pi^2} \right| , \quad (4)$$

where

$$G \equiv \left[1 - (-1)^n \cos\left(\frac{L_w - L_b}{L_w + L_b} n\pi \right) \right]^{1/2} \quad (5)$$

for the miniband edges above (+) and below (−) the nth miniband gap, respectively. To obtain the expression for $E_n^{\pm}$ a small effective-mass difference $(m_b - m_w)$ is assumed in addition to a small offset V_{off}. Similarly the superlattice effective masses m_{SL} at the miniband edges are found to be

$$m_{\text{SL}} = \frac{m_w L_w + m_b L_b}{L_w + L_b} \left[1 + \frac{L_w^2 L_b^2 (m_b - m_w)}{3\hbar^2 (L_w + L_b)^2} V_{\text{off}} \right] \quad (6)$$

for the lowest miniband edge and

$$m_{\text{SL}}^{\pm} = \pm \frac{G}{2\sqrt{2}\pi n} \left| (m_b - m_w) + \frac{V_{\text{off}} (m_w + m_b)^2 (L_w + L_b)^2}{2\hbar^2 n^2 \pi^2} \right| \quad (7)$$

for the edge above (+) and below (−) the nth miniband gap. For small V_{off}, i.e. for not too narrow minibands, the approximate expressions (3)–(7) give the parameters necessary in the nested effective-mass theory where the spatially varying superlattice potential inside each superlattice section of the SOS has vanished from the effective-mass equation.

For large V_{off} the minibands are narrow, and the approximate expressions above are less useful, but the notion of position-dependent minibands still is. With narrow minibands there will be large energy intervals which do not correspond to minibands in either of the superlattices made by the building blocks of the SOS. The Saxon-Hutner conjecture[22] states that an energy level which is forbidden in the infinite one-dimensional lattice formed of pure type-A localized potentials and in that formed by pure type-B localized potentials is also forbidden in any arbitrary substitutional alloy of A and B. This conjecture has only been proved rigorously for equally spaced δ-well potentials,[23] and examples of potentials for which the conjecture does not hold have been found.[24] We believe that the conjecture is applicable to the SOS structures we presently consider. This surmise is based on numerical checks of the conjecture for a variety of representative SOS structures. Even if examples of violations of the conjecture are found, the number of such states would probably be small, and their presence would not change the main picture. Assuming the validity of the conjecture for the present SOS systems, the position of the SOS states can be tailored by adjusting the positions of the minibands in the constituent superlattices, since energies which correspond to gaps in both superlattices also correspond to a gap in the SOS. Although the approximate expressions (3) and (4) for the miniband edges are inaccurate for large V_{off}, they still offer guidance in how the miniband edges depend on material parameters. This is helpful even if the exact expression (2) must be solved numerically to obtain accurate miniband edges.

The absorption coefficient $\alpha(E)$ for light polarized in the x direction for SOS structures is found by evaluating[25]

$$\alpha(E) = \frac{4\pi^2 e^2}{nc\Omega} \frac{\hbar}{E} \times \sum_{i,f} \left| \left\langle i \left| \frac{-i\hbar}{2} \left(\frac{1}{m(x)} \frac{d}{dx} + \frac{d}{dx} \frac{1}{m(x)} \right) \right| f \right\rangle \right|^2 \times \delta(E_f - E_i - E) , \quad (8)$$

where n is the refractive index and Ω is the sample volume. The eigenvalues (E_i and E_f) and the corresponding wave functions ($|i\rangle$ and $|f\rangle$) are found by solving Eq. (1). The sum over i (f) in Eq. (8) goes over all states with "total" energies less (larger) than the Fermi energy E_F. This "total" energy is the sum of the energy found by solving Eq. (1) and the kinetic energy in the yz plane ($\hbar^2 k_{\parallel}^2 / 2m_{\parallel}$). For the inverse parallel effective mass $1/m_{\parallel}$ we use a simple weighted average of the constituent inverse effective masses.[21] For simplicity we neglect in the following the contribution to the offset potential for nonzero $k_{\parallel}$ due to position-dependent effective masses.[19]

To get an indication of how robust the desirable features of the SOS structure are to disorder in the layer thicknesses,[18] we also consider structures where the layer widths λ are Gaussian distributed, i.e.,

$$P(\lambda) = \frac{1}{\sqrt{2\pi}\Delta L} e^{-(\lambda - L)^2 / 2\Delta L^2} , \quad (9)$$

where L is the average width. The layers with Gaussian distributed widths are stacked upon one another. This is known as cumulative disorder.[26] For disordered structures the periodicity is broken and a finite sample (with hard-wall sample boundaries) is used for computation.

III. APPLICATION TO CONVENTIONAL SUPERLATTICES

Recently Gunapala *et al.* demonstrated an IP using lattice-matched $In_{0.53}Ga_{0.47}As/InP$ with a higher responsivity than for similar $GaAs/Al_xGa_{1-x}As$ detectors.[12] To achieve this the well width was chosen so that the first excited state was close to the top of the InP barrier, a choice which has been claimed to give particularly high responsivities.[11,27] The fulfillment of this requirement fixes the well width and thus the operating frequency ($\sim$ 160 meV) of the IP. To get other operating frequencies other $In_xGa_{1-x}As$ alloys must be chosen for the well material,[12] but this will introduce strain and new complications may arise. With a SOS structure, however, the operating frequency can be tailored using lattice-matched $In_{0.53}Ga_{0.47}As$ and InP only. An example is shown in Fig. 2(a), where the sections of the superlattices

with the highest zeroth miniband edge E_0 are so wide that the electrons in the ground state predominantly reside in the superlattice sections with the lowest E_0. In the nested effective-mass picture their states can be viewed as quantum-well states. Since high responsivities have been achieved in conventional quantum-well detectors when the final state of the absorbing transition is energetically close to the barrier, we have in our SOS example correspondingly selected the well and barrier widths so that the second SOS miniband is close to the zeroth miniband edge of the "barrier" superlattice. For the material parameters we use $m_{In_{0.53}Ga_{0.47}As} = 0.041m_0$, $m_{InP} = 0.079m_0$, $E_{InP} - E_{In_{0.53}Ga_{0.47}As} = 242$ meV,[28] and the widths are given in Fig. 2(a). In Fig. 2(a) we also give the values for the four lowest SOS miniband edges found by solving the exact effective-mass equation (1) numerically and by using the simpler nested effective-mass scheme with superlattice effective masses and miniband offsets taken from Eqs. (3) and (6). A very good agreement is observed between the exact solution for the usual effective-mass approximation and the nested effective-mass approximation. When the width of the sections of "barrier" superlattice is increased, the first and second SOS minibands approach discrete levels. In this limit the nested effective-mass theory predicts the transition energy between the ground and first excited quantum-well state $E_{0\to1}$ to be 88.6 meV in near perfect agreement with the exact value $E_{0\to1} = 88.2$ meV found by solving Eq. (1).

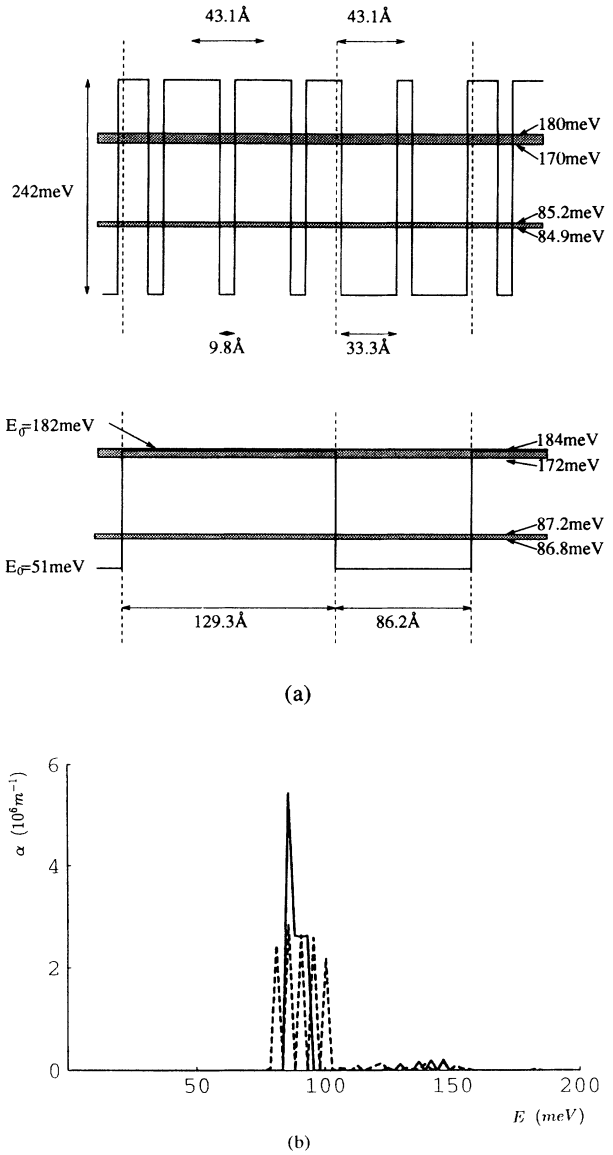

FIG. 2. (a) A 3×2 SOS structure made of $In_{0.53}Ga_{0.47}As$ (well material) and InP (barrier material). The energies of the four lowest SOS miniband edges, found by solving Eq. (1), are shown in the upper drawing. The lower drawing shows the same SOS structure in the nested effective-mass picture with the lowest miniband edge E_0 of the constituent superlattices marked. Here the displayed values for the SOS miniband edges are found by solving Eq. (2) with material parameters found from Eqs. (3) and (6). (b) The absorption spectra for the 3×2 SOS structure in (a) for an ordered (solid) and a disordered structure (dotted). The Fermi level E_F has been set at 145 meV. In the disordered structure the well widths are Gaussian distributed with $\Delta L_W = 3$ Å.

The absorption spectra for both an ordered and a disordered SOS structure are shown in Fig. 2(b). The curves are obtained by grouping the absorbing transitions into small energy intervals ($\Delta E = 1\%$ of V_{off}, i.e., $\sim$ 2.5 meV), replacing the absorption strength by a rectangle of width ΔE with the same integrated absorption strength, and then finally interpolating this "histogram." We have used the value $n = 3.4$ for the refractive index.[29] The Fermi level is set at 145 meV, which corresponds to an electron density of $6 \times 10^{17}\text{cm}^{-3}$. Since the disordered system is not periodic, we have considered a structure consisting of six "barrier"-superlattice sections and five "well"-superlattice sections with a total length of 1200 Å. Although the details in the shape of the absorption peak depend on the size of the system considered, the important features like peak position and spectral width are essentially independent of size. In the disordered structure the well widths are Gaussian distributed [Eq. (9)] with $\Delta L_W = 3$ Å. Even with this substantial disorder compared to currently obtainable sample qualities,[13] the important absorption peak centered at $\sim$ 88 meV is still strong, and this increases the confidence in the feasibility of the SOS structures. We note that the robustness of the peak to disorder stands in contrast to the disorder effect on the minigap in conventional superlattices.[18]

To optimize the IP performance for this particular system it may be better to substitute the "barrier" superlattice with pure InP and tune the operating frequency with the parameters of the "well" superlattice. Then the photoexcited electrons would be above the InP barrier, and tunneling would not be required to reach the contact. In addition the alloy scattering in the barrier would probably be reduced since InP is a binary alloy while $In_{0.53}Ga_{0.47}As$ is a ternary alloy. Moreover, the scattering due to layer-width disorder would be reduced.

Gunapala, Levine, and Chand[3] recently demonstrated an efficient $GaAs/Al_xGa_{1-x}As$ photoconductor based on transitions between bound and continuum superlattice

minibands [see Fig. 3(a)]. Although a large responsivity was found, a negative side effect of the narrow barriers, with the corresponding non-negligible width of the lowest miniband, was a significant dark tunneling current. A SOS structure as shown schematically in Fig. 3(b) is expected to have performance characteristics similar to those of the superlattice in Fig. 3(a), except that the dark current will be reduced. With the lowest minibands of the two constituting superlattices chosen to be nonoverlapping, the dark current due to tunneling will be substantially reduced since the two sections act as each other's barrier as far as the ground state is concerned. Simultaneously the minibands in the continuum can be chosen to have the same position and width and, thus, resemble a continuum miniband in conventional superlattices. Thus, similar absorption spectra and a similarly good collection of photoelectrons are expected.

A variation of this is a SOS structure where the lowest miniband in the "barrier" superlattice overlaps with the second miniband of the "well" superlattice [Fig. 4(a)]. The spectral width of the absorption is essentially governed by the width of these minibands, and the dark tunneling current can be reduced to a minimum by choosing wide sections of "barrier" superlattices. An example of such a SOS structure, made with GaAs and $Al_{0.3}Ga_{0.7}As$, is given in Fig. 4(a). The corresponding absorption spectra for both an ordered and a disordered structure are shown in Fig. 4(b). For the material parameters we use $m_{GaAs} = 0.07m_0$, $m_{Al_{0.3}Ga_{0.7}As} = 0.088m_0$, $E_{Al_{0.3}Ga_{0.7}As} - E_{GaAs} = 243$ meV, and $n = 3.4$ for the refractive index.[19,29,30] The width of the absorbing peak is, for the ordered structure, observed to correspond to the width of the absorbing minibands. In the disordered structure the well widths are Gaussian distributed with $\Delta L_W = 3$ Å. Although the spectral width is slightly larger for the disordered case, the strong absorbing peak has not vanished.

Yu, Li, and Ho[14] recently demonstrated strong intersubband absorption using a quantum-well-like structure where an $In_{0.52}Al_{0.48}As/In_{0.53}Ga_{0.47}As$ short-period superlattice replaced the barrier while pure $In_{0.53}Ga_{0.47}As$ was used in the well. They claimed that the multiple bound-to-miniband transitions in such structures would give a significantly larger integrated absorption strength (five times larger in their example) compared to a single bound-to-bound transition in a conventional quantum well. We found their claim to be unsubstantiated by calculation. Even though the number of active final states in the bound-to-miniband transition case is larger than in the single bound-to-bound transition case, the optical strength of each transition is correspondingly smaller so that the integrated absorption strength is about the same. We have confirmed this by direct calculations, but it also follows directly from the sum rule, which states that the integrated absorption strength essentially only depends on the number of absorbing electrons.[31] Despite

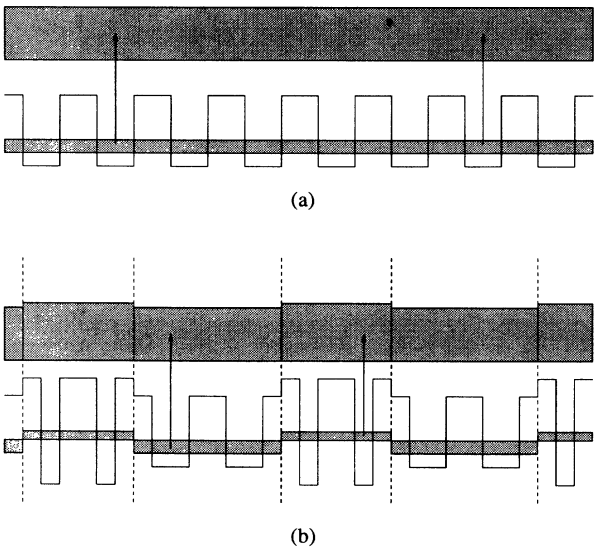

FIG. 3. (a) Schematic drawing of the miniband structure in conventional bound-to-continuum superlattice miniband photodetectors. (b) Schematic drawing of an alternative device, using the SOS concept, predicted to have a much smaller dark current due to tunneling of the electrons in the lowest miniband.

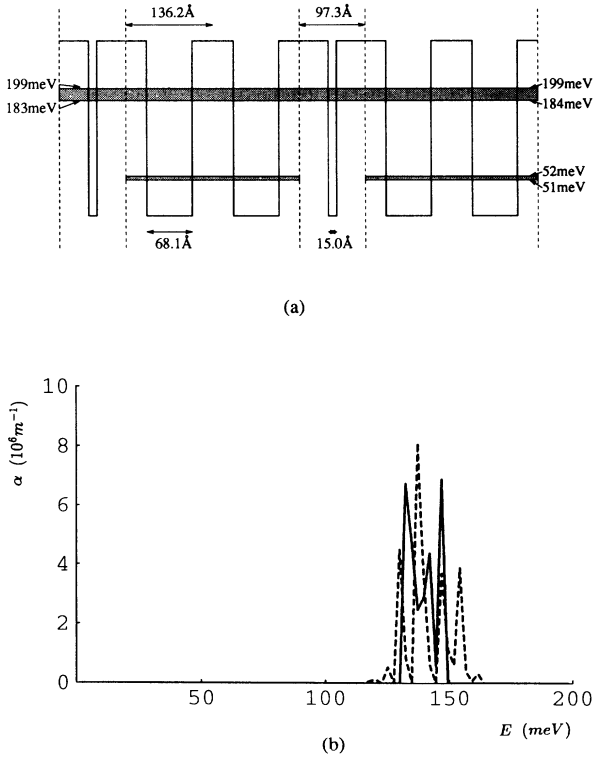

FIG. 4. (a) A 1×2 SOS structure made of GaAs and $Al_{0.3}Ga_{0.7}As$. The miniband edges, found from Eq. (2), of the constituent superlattices are shown. (b) The corresponding absorption spectra for a sample with four sections of "barrier" superlattice and three sections of "well" superlattice for both an ordered (solid) structure and a disordered (dotted) structure. In the disordered structure the well widths are Gaussian distributed with $\Delta L_W = 3$ Å. The Fermi level is at 146 meV.

their potential for tailoring desirable characteristics of devices, the SOS structures cannot circumvent this sum rule.

IV. APPLICATION TO LATERAL SUPERLATTICES

As a final example of application of the SOS concept we consider lateral superlattices. Stormer *et al.*[17] recently fabricated a two-dimensional electron gas with a lateral potential by modulation-doped molecular-beam-epitaxial overgrowth on the cleaved edge of a $GaAs/Al_{0.24}Ga_{0.76}As$ compositional superlattice. The materials were chosen so that the electron gas was predominantly located in a thin layer on the superlattice side of the boundary between the superlattice and the $Al_{0.33}Ga_{0.67}As$ capping slab. A nice feature of this structure is that light which arrives perpendicular to the capping slab has polarization in the superlattice direction. This allows for easier collection of light and is thus an advantage in device construction. By assuming the independent-particle picture to be valid and the electrons to reside in the superlattice only, the minibands of the structure are easily determined. With GaAs as well material and $Al_{0.24}Ga_{0.76}As$ as barrier material the barrier height is 195 meV.[30] In the structure of Stormer *et al.* the well width was 71 Å while the barrier width was 31 Å. With $m_{GaAs} = 0.07m_0$ and $m_{Al_{0.24}Ga_{0.76}As} = 0.084m_0$ (Ref. 19) one finds the first miniband to stretch from 38 to 55 meV while the second miniband covers the energies between 144 and 219 meV. Stormer *et al.* measured an electron density of 3×10^{11} cm^{-2}, which corresponds to a Fermi level at $\sim$ 46 meV, i.e., in the middle of the lowest miniband. Since the minibands of this structure are wide and the Fermi level lies in the middle of the first miniband, it is not to be expected that an absorption spectrum would reveal clear signatures of the existence of these minibands. This surmise has been confirmed by a calculation. To obtain signatures of the existence of minibands, a lateral SOS structure as shown in Fig. 5(a), which utilizes the same alloys, is a better alternative. This structure is designed to have the second miniband of the "well" superlattice aligned with the first miniband of the "barrier" superlattice [Fig. 5(b)]. The corresponding absorption spectra for an ordered and a disordered structure (with $\Delta L_W = 3$ Å) are shown in Fig. 5(c). The Fermi level is set at $E_F = 47$ meV in order to have the same electron density as in the structure of Stormer *et al.*, namely 3×10^{11} cm^{-2}. The curves in Fig. 5(c) correspond to the absorption coefficient of a 100-Å-wide layer (in the z direction) in the SOS structure (at the cleaving edge), which has been presupposed to contain all electrons in the 2D electron gas.

Our calculational scheme does not include electron-electron interactions and may give quantitatively inaccurate transition energies and wave functions. However, we do not believe that more elaborate self-consistent calculation schemes would change the important conclusion regarding the advantages of using SOS structures. The narrow absorption peaks, also present with substantial

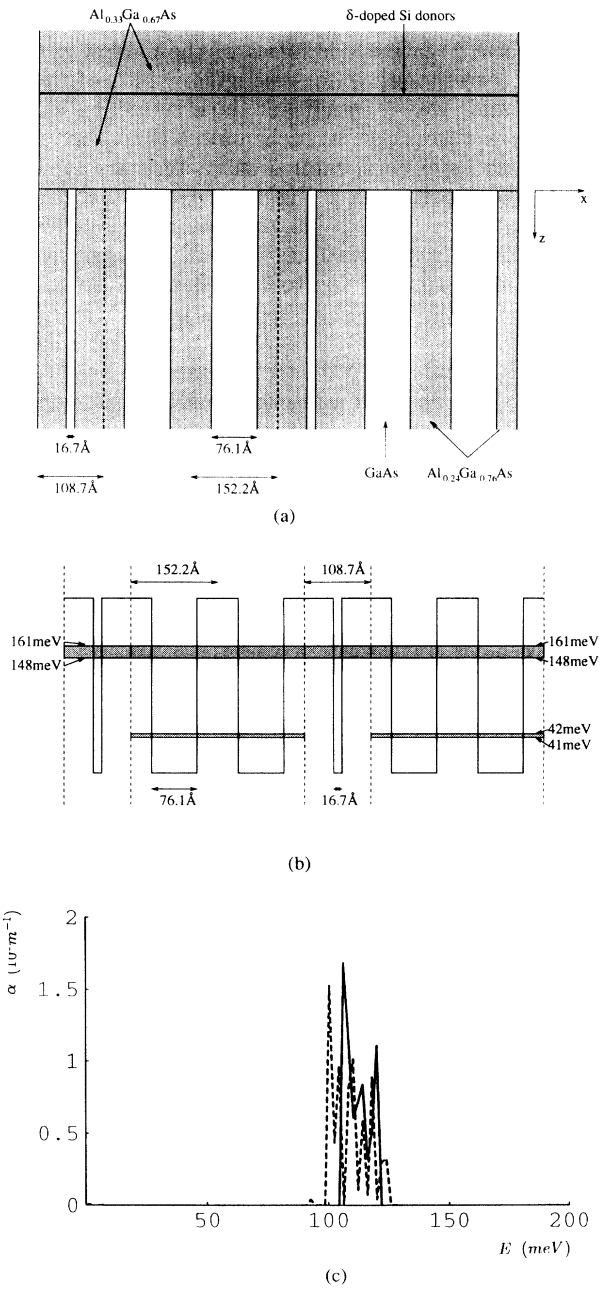

FIG. 5. (a) A 1×2 lateral SOS structure based on the concept of Stormer *et al.* (Ref. 17). The 2D electrons which feel the SOS potential are located in a thin layer on the SOS side of the interface between the SOS structure and the $Al_{0.33}Ga_{0.67}As$ capping slab. (b) The conduction-band profile of the lateral SOS structure in (a). The miniband edges of the constituent superlattices are shown. (c) The corresponding absorption spectra for a sample with four sections of "barrier" superlattice and three sections of "well" superlattice are shown for both an ordered (solid) structure and a disordered (dotted) structure with Gaussian distributed well widths with $\Delta L_W = 3$ Å. The Fermi level is at 47 meV, which corresponds to an electron density of 3×10^{11} cm^{-2}. The curves correspond to the absorption coefficient of a 100-Å-wide layer (in the z direction) in the SOS structure, which has been assumed to contain all electrons of the 2D electron gas.

disorder, indicate that measurements on a lateral SOS structure may demonstrate the presence of minibands in lateral superlattices.

V. SUMMARY AND CONCLUSION

In this paper we have introduced superlattices of superlattices (SOS's) as a concept for tailoring infrared optical properties of semiconductor heterostructures. The SOS structures can be tailored to give desirable absorption characteristics, such as operating frequency and spectral width, to control dark current, and to assure transport of photoexcited electrons to the contacts. The nested effective-mass approximation has proven to be a simple and versatile tool for describing the SOS states. We have applied the SOS concept to both conventional binary superlattices and binary lateral superlattices and demonstrated how desirable absorption spectra can be obtained. Since the SOS structures are as easy to grow as regular superlattice structures and since the nested effective-mass approximation offers a simple and transparent theoretical description, we believe that the SOS concept will be very useful for future device fabrication.

ACKNOWLEDGMENTS

G.T.E. acknowledges the Royal Norwegian Council for Science and the Humanities (NAVF) for financial support. L.J.S. was supported in part by NSF Grant No. DMR 91-17298.

[1]B.F. Levine, K.K. Choi, C.G. Bethea, J. Walker, and R.J. Malik, Appl. Phys. Lett. **50**, 1092 (1987).
[2]B.F. Levine, C.G. Bethea, K.K. Choi, J. Walker, and R.J. Malik, J. Appl. Phys. **64**, 1591 (1988).
[3]S.D. Gunapala, B.F. Levine, and N. Chand, J. Appl. Phys. **70**, 305 (1991).
[4]A. Kastalsky, T. Duffield, S.J. Allen, and J. Harbison, Appl. Phys. Lett. **52**, 1320 (1988).
[5]O. Byungsung, J.W. Choe, M.H. Francombe, K.M.S.V. Bandara, D.D. Coon, Y.F. Lin, and W.J. Takei, Appl. Phys. Lett. **57**, 503 (1990).
[6]B.F. Levine, C.G. Bethea, G. Hasnain, J. Walker, and R.J. Malik, Appl. Phys. Lett. **53**, 296 (1988).
[7]B.F. Levine, G. Hasnain, C.G. Bethea, and N. Chand, Appl. Phys. Lett. **54**, 2704 (1989).
[8]S.D. Gunapala, B.F. Levine, L. Pfeiffer, and K. West, J. Appl. Phys. **69**, 6517 (1991).
[9]E. Rosencher, E. Martinet, F. Luc, Ph. Bois, and E Böckenhoff, Appl. Phys. Lett. **59**, 3255 (1991).
[10]A. Köck, E. Gornik, G. Abstreiter, G. Böhm, M. Walther, and G. Weimann, Semicond. Sci. Technol. **6**, C128 (1991).
[11]A.G. Steele, H.C. Liu, M. Buchanan, and Z.R. Wasilewski, Appl. Phys. Lett. **59**, 3625 (1991).
[12]S.D. Gunapala, B.F. Levine, D. Ritter, R. Hamm, and M.B. Panish, Appl. Phys. Lett. **58**, 2024 (1991).
[13]D. Ritter, R.A. Hamm, M.P. Panish, J.M. Vandenberg, D. Gershoni, S.D. Gunapala, and B.F. Levine, Appl. Phys. Lett. **59**, 552 (1991).
[14]L.S. Yu, S.S. Li, and P. Ho, Appl. Phys. Lett. **59**, 2712 (1991).
[15]R.P.G. Karunasiri, J.S. Park, and K.L. Wang, Appl. Phys. Lett. **59**, 2588 (1991).
[16]H. Hertle, G. Schuberth, E. Gornik, G. Abstreiter, and F. Schäffler, Appl. Phys. Lett. **59**, 2977 (1991).
[17]H.L. Stormer, L.N. Pfeiffer, K.W. Baldwin, K.W. West, and J. Spector, Appl. Phys. Lett. **58**, 726 (1991).
[18]L.J. Sham, Appl. Phys. Lett **59**, 2010 (1991).
[19]G. Bastard, *Wave Mechanics Applied to Semiconductor Heterostructures* (Les Editions de Physique, Les Ulis, France, 1988).
[20]See, for example, G.T. Einevoll, P.C. Hemmer, and J. Thomsen, Phys. Rev. B **42**, 3485 (1990).
[21]G.T. Einevoll and P.C. Hemmer, Semicond. Sci. Technol. **6**, 590 (1991).
[22]D.S. Saxon and R.A. Hutner, Philips Res. Rep. **4**, 81 (1949); B.Y. Tong, Phys. Rev. **175**, 710 (1968).
[23]J.M. Luttinger, Philips Res. Rep. **6**, 303 (1951).
[24]E.H. Kerner, Phys. Rev. **95**, 687 (1954).
[25]This expression, which is valid for position-dependent effective masses, is a generalization of the standard expression for the absorption when the effective mass is constant [see, e.g., G. Bastard, *Wave Mechanics Applied to Semiconductor Heterostructures* (Les Editions de Physique, Les Ulis, France, 1988)]. The generalization follows from replacing $\mathbf{p}$ with $\mathbf{p}-e\mathbf{A}$ in the kinetic operator in Eq. (1) and collecting terms which are linear in the vector potential $\mathbf{A}$.
[26]W. Sevenhans, M. Gijs, Y. Bruynseraede, H. Homma, and I. Schuller, Phys. Rev. B **34**, 5955 (1986).
[27]D.D. Coon and R.P.G. Karunasiri, Appl. Phys. Lett. **45**, 649 (1984).
[28]D. Gershoni, H. Temkin, and M.B. Panish, Phys. Rev. B **38**, 7870 (1988).
[29]C.M. Wolfe, N. Holonyak, and G.E. Stillman, *Physical Properties of Semiconductors* (Prentice-Hall, Englewood Cliffs, NJ, 1989).
[30]For the conduction-band offset potential we use $V_c(x) = 0.65 \times 1247 \times x$ meV. The 65% rule is taken from R.C. Miller, D.A. Kleinman, and A.C. Gossard, Phys. Rev. B **29**, 7085 (1984). For the difference in band gap we use the room-temperature (300 K) relation $1247 \times x$ meV obtained by H.C. Casey and M.B. Panish, *Heterostructure Lasers* (Academic, New York, 1978).
[31]The sum rule, which, for example, can be found in C. Kittel, *Introduction to Solid State Physics* (Wiley, New York, 1976), is derived assuming a constant effective mass.

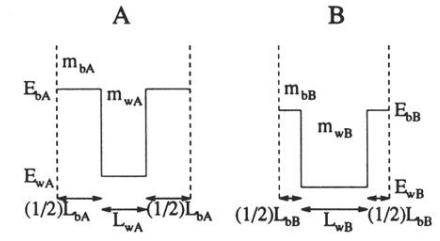

(a)

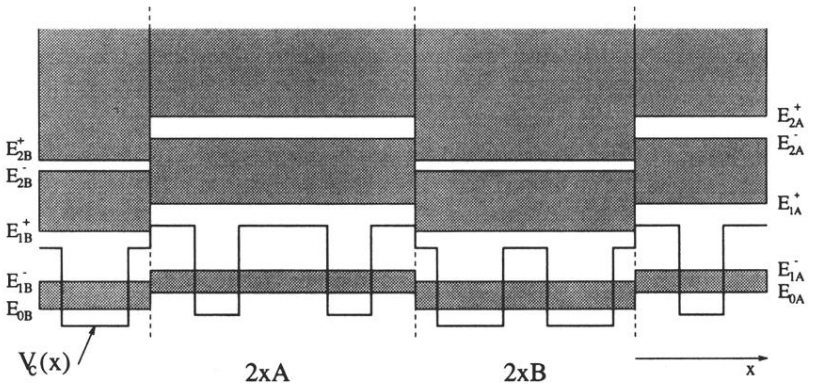

(b)

FIG. 1. The basic building blocks A and B (a) put together in a 2×2 SOS structure (b). In (b) the conduction-band edge profile $V_c(x)$ and the lowest minibands of the constituent superlattices are shown. The five lowest miniband edges of the two superlattices are marked.

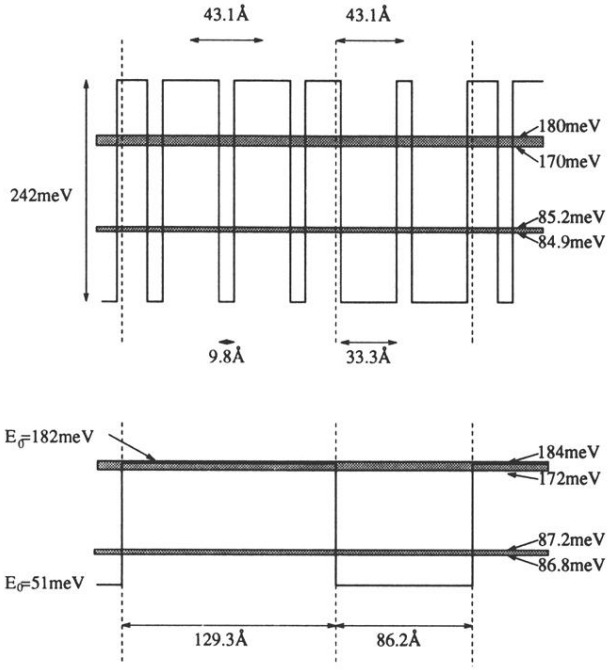

(a)

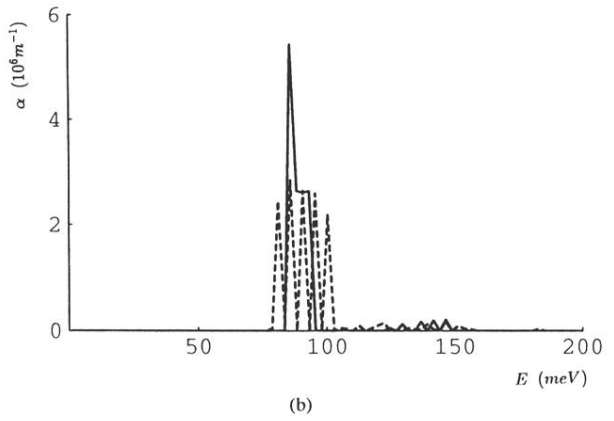

(b)

FIG. 2. (a) A 3×2 SOS structure made of $In_{0.53}Ga_{0.47}As$ (well material) and InP (barrier material). The energies of the four lowest SOS miniband edges, found by solving Eq. (1), are shown in the upper drawing. The lower drawing shows the same SOS structure in the nested effective-mass picture with the lowest miniband edge E_0 of the constituent superlattices marked. Here the displayed values for the SOS miniband edges are found by solving Eq. (2) with material parameters found from Eqs. (3) and (6). (b) The absorption spectra for the 3×2 SOS structure in (a) for an ordered (solid) and a disordered structure (dotted). The Fermi level E_F has been set at 145 meV. In the disordered structure the well widths are Gaussian distributed with $\Delta L_W = 3$ Å.

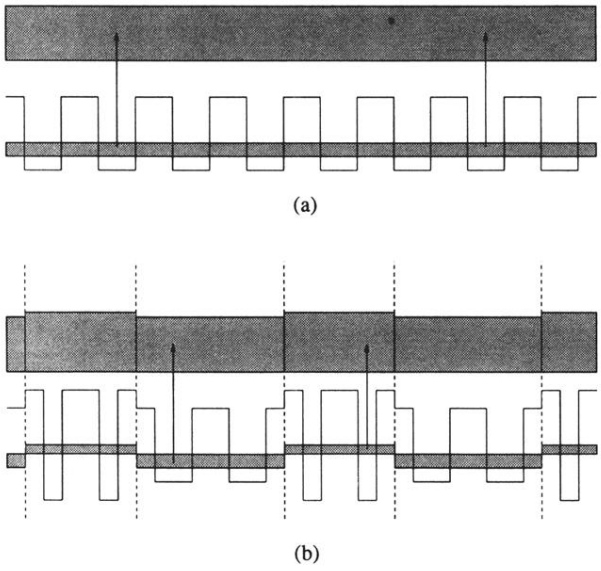

FIG. 3. (a) Schematic drawing of the miniband structure in conventional bound-to-continuum superlattice miniband photodetectors. (b) Schematic drawing of an alternative device, using the SOS concept, predicted to have a much smaller dark current due to tunneling of the electrons in the lowest miniband.

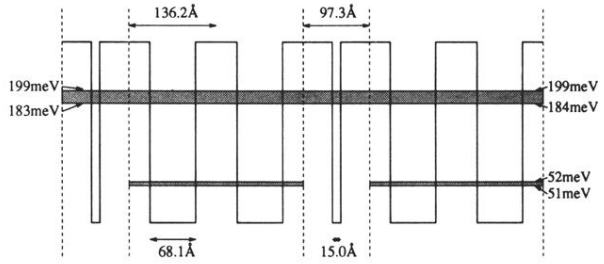

(a)

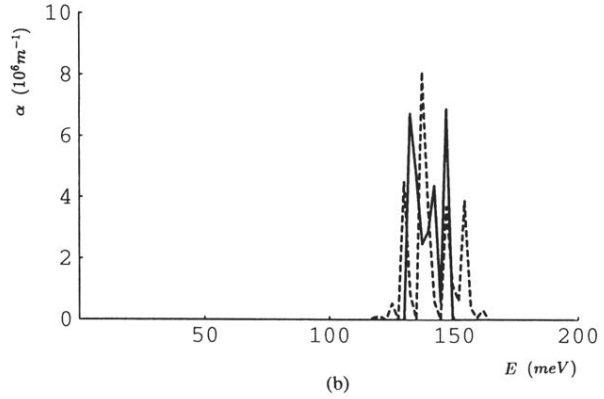

(b)

FIG. 4. (a) A 1×2 SOS structure made of GaAs and $Al_{0.3}Ga_{0.7}As$. The miniband edges, found from Eq. (2), of the constituent superlattices are shown. (b) The corresponding absorption spectra for a sample with four sections of "barrier" superlattice and three sections of "well" superlattice for both an ordered (solid) structure and a disordered (dotted) structure. In the disordered structure the well widths are Gaussian distributed with $\Delta L_W = 3$ Å. The Fermi level is at 146 meV.

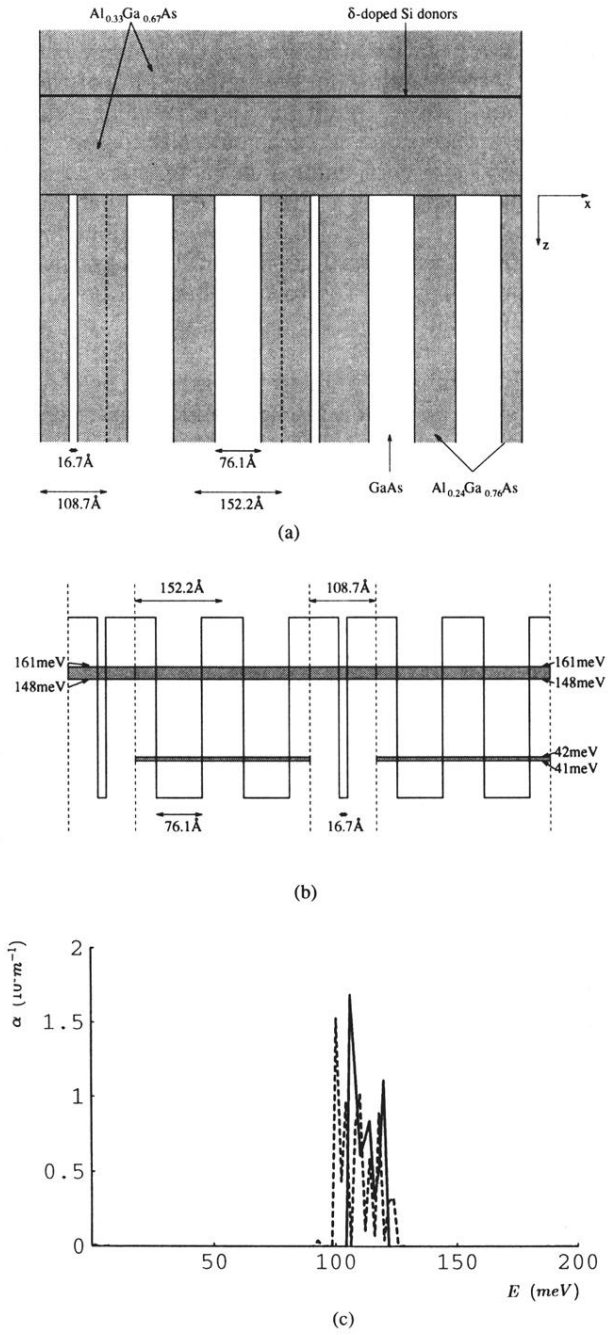

FIG. 5. (a) A 1×2 lateral SOS structure based on the concept of Stormer *et al.* (Ref. 17). The 2D electrons which feel the SOS potential are located in a thin layer on the SOS side of the interface between the SOS structure and the $Al_{0.33}Ga_{0.67}As$ capping slab. (b) The conduction-band profile of the lateral SOS structure in (a). The miniband edges of the constituent superlattices are shown. (c) The corresponding absorption spectra for a sample with four sections of "barrier" superlattice and three sections of "well" superlattice are shown for both an ordered (solid) structure and a disordered (dotted) structure with Gaussian distributed well widths with $\Delta L_W = 3$ Å. The Fermi level is at 47 meV, which corresponds to an electron density of 3×10^{11} cm^{-2}. The curves correspond to the absorption coefficient of a 100-Å-wide layer (in the z direction) in the SOS structure, which has been assumed to contain all electrons of the 2D electron gas.